First Results of Cloud Retrieval from Geostationary Environmental Monitoring Spectrometer

Bo-Ram Kim [1,2], Gyuyeon Kim [3], Minjeong Cho [3], Yong-Sang Choi [3, *], and Jhoon Kim [4]

[1]Satellite Application Division, National Satellite Operation and Application Center, Korea Aerospace Re-search Institute, Daejeon 34133, Republic of Korea
[2]Department of Atmospheric Science and Engineering, Ewha Womans University, Seoul 03760, Republic of Korea
[3]Department of Climate and Energy Systems Engineering, Ewha Womans University, Seoul 03760, Republic of Korea
[4]Department of Atmospheric Science, Yonsei University, Seoul 03722, Republic of Korea

Correspondence to: Yong-Sang Choi (ysc@ewha.ac.kr)

Abstract. This paper introduces a cloud retrieval algorithm for the Geostationary Environmental Monitoring Spectrometer (GEMS), the first environmental geostationary orbit satellite, and validates its cloud products by comparing them with those produced by other instruments (OMI, TROPOMI, AMI, and CALIOP). The GEMS cloud products are corrected for the impact of clouds on the retrieval of atmospheric components, using the O_2-O_2 absorption band to retrieve the effective cloud fraction and cloud centroid pressure. The performance of the GEMS retrieval algorithm was similar to that of the OMI instrument. We analyzed the cloud retrieval characteristics for air pollution, typhoons, and fog in the East Asia region to evaluate whether GEMS cloud data can accurately represent various cloud features. The validation results provide a basis for future improvements of the GEMS cloud retrieval algorithm.

1 Introduction

Since the deployment of the Total Ozone Mapping Spectrometer (TOMS) in 1978 to monitor changes in the ozone layer, atmospheric composition has been monitored continuously by remote sensing satellites. TOMS was followed by the Ozone Monitoring Instrument (OMI), Global Ozone Monitoring Experiment (GOME), SCanning Imaging Absorption spectroMeter for Atmospheric CHartographY (SCIAMACHY), and the recent the Tropo-spheric Monitoring Instrument (TROPOMI) (Hsu et al., 1997; Burrows et al., 1999; Bovensmann et al., 1999; Levelt et al., 2006; Veefkind et al., 2012). Other instruments such as the Greenhouse Gas Satellite (GHGSat), Greenhouse gases Observing SATellite (GOSAT), and the Orbiting Carbon Observatory-2 (OCO-2) have been launched recently to gather data on greenhouse gases as part of global efforts to understand climate change (Yoshida et al., 2011; Frankenberg et al., 2015; Jervis et al., 2021). Satellite-based monitoring of the atmosphere has been extended to include data for other air pollutants, including nitrogen dioxide, sulfur dioxide, and aerosols, in addition to ozone, using spectrometers that can monitor spectral regions within the ultraviolet (UV)-visible (Vis) range of 240–790 nm at spectral resolutions of 0.2–0.4 nm depending on the instrument (Hsu et al., 1997; Burrows et al., 1999; Bovensmann et al., 1999; Levelt et al., 2006; Veefkind et al., 2012). Satellites now monitor global warming by measuring greenhouse gases such

as carbon dioxide and methane using spectrometers in the near-infrared and shortwave-infrared regions (Yoshida et al., 2011; Frankenberg et al., 2015; Jervis et al., 2021).

To obtain precise data on atmospheric composition, it is necessary to accurately estimate the beam path length of the radiation that reaches the satellite. The beam path length begins with the emission of solar energy from the sun and follows it as it reflected from Earth before reaching the satellite and is also a function of geometric factors such as solar zenith angle (SZA) and viewing zenith angle (VZA). Cloud reflectance is typically greater than that of most surfaces (excluding snow and ice) and takes place above the surface of the Earth. Cloud pixels have higher reflectance values compared with clear-sky pixels, and the beam path length is shorter, blocking the path from atmospheric components below, which can result in errors in observations of atmospheric variables (Hong et al., 2017; Chimot et al., 2018). To obtain accurate measurement of concentrations of atmospheric components, it is therefore necessary to evaluate and quantify the effects of clouds.

A cloud can exhibit significant spatiotemporal variability, and its characteristics can vary widely depending on the instrument. To accurately measure atmospheric components, it is first necessary to obtain real-time cloud information that reflects the characteristics of the satellite's instruments. Instruments that monitor the atmospheric environment use their own algorithms to extract information on clouds. In previous studies, spectral bands that reveal phenomena involving gases with relatively constant proportions in the dry atmosphere, such as those associated with rotational Raman scattering (RRS) (Joiner et al., 2006; Vasilkov et al., 2008), O_2-O_2 absorption (Acarreta et al., 2004; Stammes et al., 2008; Veefkind et al., 2016; Vasilkov et al., 2018), and O_2-A absorption (Wang et al., 2008; Wang et al., 2014; Loyola et al., 2018; Compernolle et al., 2021; Yang et al., 2021; Taylor et al., 2021), have been used for cloud retrieval. The GOME, SCIAMACHY, and TROPOMI instruments use the O_2-A band to retrieve cloud information, while the OMI (without the O_2-A band) retrieves information using two methods: Raman scattering and the O_2-O_2 absorption band (Acarreta et al., 2004; Joiner et al., 2006; Stammes et al., 2008; Vasilkov et al., 2008; Wang et al., 2008; Vasilkov et al., 2018; Veefkind et al., 2016; Wang et al., 2018; Loyola et al., 2018; Compernolle et al., 2021). The GOSAT and GHGSat instruments make use of the O_2-A band to monitor clouds and aerosols, perform cloud screening, and make cloud-cover estimates to gauge the influence of clouds. The OCO-2 satellite also monitors the O_2-A band, which is used for cloud screening (Taylor et al., 2011; Yang et al., 2021).

GEMS, which was launched in 2020, was the first environmental monitoring satellite in geostationary Earth orbit (GEO) (Kim et al., 2020). GEMS measures levels of ozone, aerosols, nitrogen dioxide, sulfur dioxide, formaldehyde, and other atmospheric constituents in the UV-Vis range over East Asia. It monitors the 300–500 nm range with a spectral resolution of 0.6 nm. As it operates in GEO, it can monitor the same field of view every hour. Previous satellites for atmospheric environmental monitoring operated primarily in a sun-synchronous orbit (SSO) while maintaining the SZA variation, whereas GEMS operates in GEO, making it essential to consider large variations in SZA and VZA. An SZA varies greatly from dawn to noon and to sunset. While satellites in SSO perform observations close to noon to take of advantage of maximum illumination of Earth, a GEO satellite operates throughout the day, from dawn to sunset. This reduces the quantity of radiation energy reaching the satellite and extends the beam path, resulting in a lower signal-to-noise ratio (Vandaele et al., 2018) and cloud retrieval errors. The development and evaluation of algorithms that take these factors into account are therefore crucial for accurate retrieval

65 of cloud data (Kim et al., 2021a). Similarly, due to the wider observation range of the VZA compared to that possible in a low Earth orbit, errors may occur due to the increase in beam path length and the increase of the VZA. As this was the first time an environmental monitoring satellite was to be operated from a GEO, studies were conducted to consider the observational characteristics due to differences in orbit (Kwon et al., 2017; Kim et al., 2018; Bak et al., 2019; Go et al., 2020; Kim et al., 2021a).

70 Here, we introduce a cloud retrieval algorithm for GEMS that takes into account the characteristics of observations made from GEO, and analyze the cloud properties retrieved from GEMS data. To ensure rapid and stable operation, the GEMS cloud retrieval algorithm was designed based on a look-up table (LUT) for the O_2-O_2 absorption band. The LUT was created assuming the range of values that can be observed by GEMS-specific conditions for variables that affect O_2-O_2 absorption, such as SZA, VZA, surface reflectance, and surface pressure. A detailed description of the algorithm is provided in Section 2.

75 To verify the performance of the algorithm, data from the OMI and TROPOMI instruments were used, and the Advanced Meteorological Imager (AMI) and Cloud-Aerosol Lidar with Orthogonal Polarization (CALIOP) cloud products were used to validate the GEMS products. The data are introduced in Section 3, and the validation results are shown and discussed in Section 4. Section 5 provides a summary and overall evaluation of the GEMS cloud retrieval algorithm.

2 Geostationary Environmental Monitoring Spectrometer (GEMS) Cloud Retrieval Algorithm

80 The GEMS is instrument is aboard the Geostationary Korea Multipurpose Satellite2B (GK2B), a geostationary craft launched by South Korea in 2020 and orbiting at 128.2°E to provide continuous atmospheric observation of East Asia. It is the first geostationary satellite to monitor the 300–500 nm range at a resolution of 0.6 nm. As a UV-Vis observation instrument, GEMS observes the East Asian region (5°S to 45°N, 75°E to 145°E) at 1 h intervals during the daytime hours (0000-0900, 2200-2300 UTC) (Kim et al., 2020). The atmospheric components that GEMS measures, such as ozone, nitrogen dioxide, sulfur dioxide,
85 formaldehyde, glyoxal, and aerosols, can be affected by clouds, leading to reduced accuracy and even making some components impossible to detect. This section introduces a cloud retrieval algorithm (Section 2.1), and defines the characteristics of clouds that can cause errors in estimates of concentration of atmospheric components (Section 2.2).

2.1 GEMS Cloud Retrieval Algorithm Description

In the GEMS cloud retrieval algorithm, the observed radiance (RAD) and irradiance (IRR) values, as well as the observation
90 geometry information, including SZA, VZA, and relative azimuth angle (RAA), and surface information such as surface pressure and surface reflectance are used as input values. During the testing of the GEMS cloud retrieval algorithm, issues with the bad pixels were identified in some areas that differed from the original design, preventing observations above 485 nm (Lee et al., 2023). The algorithm was therefore developed using the 460–485 nm range instead of the originally planned 460–490 nm range as input data for cloud retrieval algorithm.

95 Cloud detection is based on the reflection and scattering properties of clouds, making it possible to determine the presence of clouds throughout the GEMS observational spectrum. Cloud pressure is quantified by changes in the absorption or filling phenomena due to variations in the beam path length caused by clouds. However, quantifying the impact of clouds when the concentration of gases can undergo significant changes can be challenging, and it is essential to select areas with minimal variation in concentrations of trace gases.

100 The GEMS cloud retrieval algorithm assumes the mixed Lambertian equivalence reflectivity (MLER) cloud model, which is the model assumption used in the OMI. Similarly, for O_2-O_2 band–based cloud retrieval by OMI, the algorithm runs a radiative transfer model with inputs of observation geometry, surface information, effective cloud fraction (ECF), and cloud centroid pressure (CCP). The algorithm uses a simulated result with a 0.6 nm interval in the 460–485 nm range to create an LUT. Detailed input values for the LUT are presented in Table 1. While OMI defines nodal points for observation geometry based

105 on the angle spacing, GEMS defines nodal points for the LUT based on the cosine value of observation geometry to ensure a linear relationship with beam path length. This approach allows for a simulation of the LUT with a superior linear interpolation scheme. For the radiative transfer simulation used to create the LUT, the Vector LInearized Discrete Ordinate Radiative Transfer (VLIDORT) NGST version (Spurr et al., 2006) was applied and the atmospheric profile as assumed based on the profiles of the Deriving Information on Surface conditions from Column and Vertically Resolved Observations Relevant to

110 Air Quality (DISCOVER-AQ) campaign (Flynn et al., 2014). The simulated radiance in the 460–485 nm range was converted to reflectance assuming the observed reflectance (R_λ) in Equation (1) is the ratio between the simulated radiance (RAD) and the irradiance (IRR).

$$R_\lambda = \frac{\pi \cdot RAD}{IRR \cdot \cos SZA} \tag{1}$$

The observed reflectance spectrum with a 0.6 nm interval in the 460–485 nm range are used as input data for the fitting method

115 based on the Differential Optical Absorption Spectroscopy (DOAS) method (Platt et al., 1979), as described by Eq. (2), which quantifies O_2-O_2 absorption.

$$ln(-R_\lambda) = C_1 + C_2 \times \lambda + N_{s,O_2-O_2} \times \sigma_{O_2-O_2} + N_{s,O_3} \times \sigma_{O_3} \tag{2}$$

where R_λ represents the 43 input observed reflectance spectra, λ is the wavelength for the 43 reflectance spectra, and C_1 and C_2 are the offset and slope of the linear component, respectively. N_s represents the slant column density (SCD), and σ refers to

120 the absorption coefficient. Before the launch of GEMS, we designed the algorithm using 460–490 nm. However, we discovered that a bad-pixels exist over 485 nm in partial area (Lee et al., 2023) during the in-orbit test of GEMS. Therefore, the fitting window was shortened for stable cloud retrieval. To account for this issue that occurs in some observation areas of GEMS, the range of wavelengths for the input data in the fitting method was adjusted to 460–485 nm.

In this study, because only the effects of O_2-O_2 and O_3 absorption were considered (Brion et al., 1998; Thalman et al., 2013),

125 only the column densities for O_2-O_2 ($N_{s, O2-O2}$) and O_3 ($N_{s, O3}$) absorption were calculated. The DOAS method separates the contribution of each gas's absorption coefficient as a weighting factor in the regions where absorption occurs, providing a linear element and the SCD of each absorption coefficient from the input reflectance spectrum. In addition, even though NO_2

absorption coefficients exist in the spectral range of the input reflectance, their effects are disregarded because the impact is negligible. In contrast, because the absorption coefficient of ozone has a peak near 480 nm, and its absorption line is prominent in the case of upper-level clouds, affecting the quantification of O_2-O_2 absorption, it should be considered and removed.

The LUT was constructed based on two intermediate products The first is the continuous reflectance (CR, R_c), which is obtained by calculating the values of linear elements obtained through DOAS using Equation (3).

$$R_c = C_1 + C_2 \times \lambda , \lambda = 477 \ nm \tag{3}$$

The second intermediate product was based on the O_2-O_2 SCD values obtained through DOAS. In the GEMS cloud retrieval algorithm (Figure 1), when the observed reflectance spectrum is provided, the intermediate products (R_c and $N_{s, O2-O2}$) are first calculated via DOAS. These intermediate products are then fed into the LUT, along with observation geometry and surface information. Through a linear interpolation process, the final products (ECF and CCP) are produced.

Although the GEMS cloud retrieval algorithm is generally similar to the OMI cloud retrieval algorithm, significant differences are in the process of generating an LUT. As already noted, the observational geometry differs from the LEO orbit because GEMS is in GEO. The VZA is constant at each location, but it varies significantly across the observation area. In contrast, SZA varies significantly across the complete observation area from sunrise to sunset. This change in SZA influences not only the calculation of reflectance, the optical path, etc., but also the variation in surface reflectance. Therefore, we simulated the RTM considering the various conditions of surface reflectance. To minimize the error of linear interpolation during the algorithm process, we therefore defined the LUT using the cosine values of the zenith angle. In addition, different models were used to generate the LUT for the two algorithms. OMI used the DAK model (Acarreta et al., 2004; Stammes et al., 2008; Veefkind et al., 2016; Vailkov et al., 2018), while GEMS used the VLIDORT NGST version (Spurr et al., 2006).

2.2 GEMS Cloud Products: Effective Cloud Fraction and Cloud Centroid Pressure

The visible and infrared regions of the electromagnetic spectrum have been commonly used for cloud-property retrieval, primarily from weather satellites. It can be challenging to measure cloud properties, such as top pressure and phase, in the UV-Vis region (Compernolle et al., 2021; Kim et al., 2019). In the GEMS cloud retrieval algorithm, cloud products are defined and produced to correct for the influence of clouds in other GEMS gaseous products over a limited spectral range. The GEMS spectral range is limited to those required to monitor specific cloud properties. We therefore assumed that the cloud is a simple reflective surface, rather than apply a mie scattering model that takes into account cloud phase and effective radius.

In the GEMS spectrum, clouds are more reflective than the Earth's surface, with the exception of snow- and ice-covered terrain, and are typically at higher altitudes than the air pollutants that GEMS is measuring. Cloud products for estimating atmospheric components should therefore correct for increased reflectance and beam path length. For the GEMS cloud retrieval algorithm, cloud products can be defined by two parameters: ECF and CCP, which are also used in the O_2-O_2 band algorithm (OMCLDO2) of OMI (Acarreta et al., 2004; Stammes et al., 2008; Veefkind et al., 2016; Vasilkov et al., 2018).

The ECF is calculated (Eq. 1) by assuming a Lambertian equivalent reflectivity (LER) of 0.8 for clouds (Accareta et al., 2004; Stammes et al., 2008), and comparing the observed reflectance (R_{obs}) at a pixel with the simulated reflectance under clear-sky (R_{clr}) and cloudy-sky (R_{cld}) conditions.

$$ECF = \frac{R_{obs} - R_{clr}}{R_{cld} - R_{clr}}$$ (3)

An LER cloud model with a reflectivity of 0.8 is assumed to represent a sufficiently thick cloud with an optical thickness of approximately 30, and the effects of reflection within the cloud and multiple scattering that occurs beneath the cloud are ignored. A cloud model that defines the radiance of observed pixels by combining clear-sky and cloudy-sky pixels, assuming a reflectance of 0.8 for clouds and independent relationships between the two types of pixels (independent pixel approximation [Acarreta et al., 2004; Stammes et al., 2008; Veefkind et al., 2016; Vasilkov et al., 2018]), is an MLER model. The pressure at which reflection occurs due to the cloud is defined as the CCP. In addition, the GEMS cloud retrieval algorithm defines a cloud radiative fraction (CRF) for the wavelengths at which the atmospheric components are retrieved, which provides a ratio of the radiance reflected by clouds to the observed radiance for the atmospheric components. Although GEMS produces three types of cloud products, this study compares only the ECF and CCP for verification with other satellites, excluding the CRF.

3 Data and Method

Four satellite datasets (Table 2) used to validate the GEMS cloud retrieval algorithm are introduced in Section 3.1 and collocation methods for comparison of each satellite's data are presented in Section 3.2. To evaluate the performance of the GEMS cloud retrieval algorithm, cloud products were produced using OMI radiance data, which are similar to the GEMS spectral resolution and cloud prototype algorithm. TROPOMI, an environmental satellite in operational since 2018, was also used to analyze the characteristics of clouds that appear during GEMS operations. AMI cloud data were gathered from the same GEO orbit but with a different definition of clouds, and CALIOP data, which are based on the vertical distribution of clouds using an active sensor, were also used for validation.

3.1 Satellite Data Used in This Study

3.1.1 OMI

In this study, the GEMS cloud retrieval algorithm was designed and developed based on the OMI cloud retrieval algorithm, which is a product based on O_2-O_2 absorption. OMI data were used as testing input to validate the algorithm. The OMI is a UV-Vis observation satellite launched in 2004 aboard Aura, a satellite in the A-train, that monitors the 270–500 nm band at intervals of 0.6 nm (Levelt et al., 2006). In addition to ozone, it also produces information on sulfur dioxide, nitrogen dioxide, and two types of cloud products: OMCLDRRS, which uses RRS near 388 nm (Joiner et al., 2006; Vasilkov et al., 2008), and OMCLDO2, which uses O_2-O_2 absorption between 460 and 490 nm (Acarreta et al., 2004; Stammes et al., 2008; Veefkind et

al., 2016; Vailkov et al., 2018). The cloud pressure is determined by the scattering and absorption characteristics that vary according to the presence of clouds in OMCLDRRS and OMCLDO2. RRS determines cloud pressure based on a phenomenon in which absorption lines formed by radiation emitted from the sun are filled by non-elastic scattering as they pass through the Earth's atmosphere. In contrast, OMCLDO2 determines cloud pressure by using the absorption characteristics generated by collisions of O_2 molecules at an almost constant mixing ratio in dry air. The RRS method produces pressure closer to cloud-top pressures compared with the O_2-O_2 method (Sneep et al., 2008; Joiner et al., 2012). Additionally, the two algorithms are effective at detecting high and low clouds, respectively, based on the characteristics of scattering and absorption used in each algorithm.

OMI data can be used to evaluate the GEMS cloud retrieval algorithm by excluding errors caused by the satellite's orbit, viewing geometry, and resolution (Park et al., 2020; Park et al., 2021). We used OMI values for RAD and IRR on randomly selected days each month in 2007 as input data for the algorithm. OMI provides surface reflectivity values for 36 channels, which are essential input data for cloud retrieval, and the GEMS cloud retrieval algorithm uses surface reflectivity values at 463 nm (adjacent to the O_2-O_2 absorption band), as does the OMI algorithm (Kleipool et al., 2008).

3.1.2 TROPOMI

The TROPOMI uses O_2-A absorption around 760 nm to produce cloud products for cloud correction (Loyola et al., 2018). The products include cloud fraction (CF), cloud-top and cloud-bottom pressure (CTP and CBP), cloud optical thickness, and various other cloud-related information. TROPOMI, a successor environmental observation satellite, is equipped with four spectrometers that observe from the UV to shortwave-infrared wavelengths, including 760 nm, and can therefore provide greater accuracy in surface and cloud products compared with GEMS. Launched in 2017, TROPOMI is in SSO (as is OMI) and has a spatial resolution of 3.5×5.5 km, which is similar to that of GEMS (Latsch et al., 2022), making it useful for testing and validating the initial GEMS results. We verified the retrieved cloud products using TROPOMI data.

TROPOMI observed the UV-Vis spectrum from its SSO and was primarily used to supply experimental and reference data for GEMS algorithms (Wang et al., 2020; Kang et al., 2020; Choi et al., 2020; Lee et al., 2020; Baek et al., 2022). TROPOMI data were also used as input for cloud products in evaluating the performance of GEMS cloud retrieval algorithms. In this study, TROPOMI provided RAD, IRR, surface reflectance, pressure, and observation geometry in an evaluation of the performance of cloud algorithms. In addition, to analyze the characteristics of clouds observed from both a GEO and an SSO, verification was performed using data observed on the same day and time (within 15 min) as the GEMS observations.

3.1.3 CALIOP

The CALIOP satellite, which is often used for qualitative cloud verification, produces a vertical feature mask (VFM) of clouds using active sensors. CALIOP is a lidar instrument that was launched in 2006 as part of the Cloud-Aerosol Lidar and Infrared Pathfinder Satellite Observation (CALIPSO) program, which observes clouds and aerosols with a significant impact on Earth's

weather and climate (Winker et al., 2009). It receives backscattered energy in bands at 532 nm and 1064 nm using three receivers and provides information on the vertical distribution of clouds and aerosols. In this study, we qualitatively compared the cloud products produced by different bands using L2-VFM data, which is a cloud-aerosol profile.

3.1.4 AMI

A comparison of the cloud-detection characteristics of meteorological and environmental satellites with different spectral ranges that operate in a GEO can provide insights into the differences in cloud properties depending on the spectral band. AMI, which produces the most diverse cloud products, including pressure, phase, optical thickness, and effective particle radius, is a meteorological sensor onboard GK2A, which monitors 16 bands between 0.5 and 13.3 μm. Because the main purpose of weather observation is to gather data on weather phenomena, multiple cloud properties are defined and produced, and cloud detection is performed simultaneously using the visible and infrared regions. CTP is based primarily on infrared channels (Kim et al., 2019), and cloud pressure in this case is less sensitive to low clouds due to reduced thermal contrast (Miller et al., 2012).

3.2 Validation Method

Validation was conducted in two ways: by evaluating the performance of the algorithm itself, excluding differences in observation sensors; and by understanding the characteristics of the cloud products produced from actual observations in GEMS. To evaluate algorithm performance, radiance data and cloud products from OMI and TROPOMI, which make observations in the UV-Vis range, were used. To compare the GEMS cloud products, TROPOMI, CALIOP, and AMI, which collects data at a time similar to that of GEMS, were used as validation instruments (Sneep et al., 2008; Kim et al., 2019).

To evaluate the performance of the GEMS cloud retrieval algorithm using OMI and TROPOMI spectral ranges, no collocation process was required. In addition, for OMI, which is based on the same cloud model as GEMS, the cloud definitions derived were identical in terms of ECF and CCP, making it possible to avoid preprocessing. However, for TROPOMI, although clouds were assumed to be LER, as was the case with GEMS, the cloud albedo (CA)was retrieved, not 0.8, and the TROPOM CF had to be converted to cloud effective amount prior to making comparisons using Equation (4) and the ECF of GEMS (Loyola et al., 2018, Latsch et al., 2022).

$$ECF = CF \times \frac{CA}{0.8} \tag{4}$$

Moreover, the cloud pressure from TROPOMI was provided as separate cloud-top and cloud-base pressures and cloud pressure (CP) with MLER assumption with retrieved CA. To compare its data with those from GEMS, which only provides cloud centroid pressure, the CP was used for validation.

To verify various cloud characteristics, cases of high aerosol concentration, typhoons, and fog were selected when GEMS, AMI, TROPOMI, and CALIOP satellites passed over the Korean Peninsula. To validate satellite data from different orbits, spatiotemporal collocation was necessary. TROPOMI and CALIOP passed the GEMS field of view between 03 and 06 UTC,

we use the entire swath to validate the GEMS products, but since most cases occurred close to the Korean Peninsula, we primarily used around the 04 UTC observation for validation. GEMS observes the Korean Peninsula at ~ 45 minute past every hour during daytime, therefore, data observed at 04:45 UTC was selected as the validation data. AMI observed the Korean Peninsula every 10 minutes, using data observed at 04:40 UTC for validation.

AMI provides cloud-detection results at a spatial resolution of 2 km × 2 km. To compare them with the ECF and to select pixels included in the GEMS observations, collocation was performed and the CF was calculated by counting the number of cloud pixels for comparison. CTP is the mean value of the cloud pixels. However, quantitative verification of the CCP from GEMS and CTP from CALIOP or AMI can be difficult, as they represent cloud pressures with different definitions. A VFM can evaluate the validity of cloud detection and estimates as it provides cloud vertical distribution. The CCP is converted to cloud centroid height (CCH) using Equation (5) for qualitative verification of cloud pressure:

$$CCH = -h_{scale} \ln\left(\frac{CCP}{p_s}\right) + h_s \qquad (5)$$

where p_s is the surface pressure and h_s is the surface altitude of GEMS pixel. A value of 7710 m was obtained by fitting the results to the atmosphere profile from the DISCOVER-AQ campaign (Flynn et al., 2014), which is a reference in the GEMS algorithm. For spatial collocation, the nearest neighbor method was used based on based on CALIOP observation pixels, which have the narrowest swath. The same method was applied to GEMS and TROPOMI collocation, along with a comparison of the nearest pixels.

4 GEMS Cloud Retrieval Algorithm Results Using OMI and TROPOMI Radiances

4.1 Comparison with OMI Clouds

The performance of the GEMS cloud retrieval algorithm was evaluated using the theoretical background of the OMI's OMCLDO2 algorithm. Using the same input data is valuable for understanding algorithm differences without error from sensor. Since OMI is the foundation of the GEMS cloud retrieval algorithm, the GEMS cloud retrieval algorithm would produce a product that is highly correlated with the OMI cloud product Figure 2 displays the characteristics of cloud products according to the season of the observational data for random days of each month in 2007. To represent the seasons, the analysis was performed using observational data for January, February, and December (DJF) for winter, March, April, and May (MAM) for spring, June, July, and August (JJA) for summer, and September, October, and November (SON) for autumn. We drew density scatterplots to compare the two products, and analyzed the correlation between them with linear regression. The x-axis represents the cloud products calculated and provided by OMI, while the y-axis represents the cloud products calculated by the GEMS cloud retrieval algorithm using OMI level-1B data as input. The top panel of Figure 1 is a density scatterplot of the ECF, while the bottom panel shows a density scatter plot of the CCP, and the solid line represents the 1:1 line.

The ECF values from GEMS and OMI were similar across the entire study area, regardless of cloud amount. The correlation coefficient was high, ranging from about 0.92 to 0.95, and the slope of the regression line was also close to 1, ranging from 0.9 to 0.94, indicating a strong agreement between GEMS and OMI. The root mean square error and mean bias error were 0.12 and −0.01, respectively, and large errors were observed primarily in areas with small ECFs. Overall, the correlation coefficient and slope for the ECF between the two satellites did not show significant seasonal differences, indicating that the algorithm design did not result in significant seasonal bias.

As with the case of the ECF, GEMS produced CCP values similar to those from OMI for the entire domain. However, many previous studies (Vasilkov et al., 2008; Sneep et al., 2008; Loyola et al., 2018; Compernolle et al., 2021) reported that the accuracy of CCP retrieval using O_2-O_2 absorption was significantly lower for areas with an ECF less than 0.2. Only pixels with an ECF greater than 0.2 were therefore validated. Both OMI and GEMS had approximately 50% of the pixels with an ECF greater than 0.2. The correlation coefficient was approximately 0.95 for all seasons, and the slope of the regression line was greater than 0.9, indicating that GEMS produced a CCP similar to those from OMI regardless of season.

Figure 3 displays the outcome of the GEMS cloud process, derived from OMI observations conducted on March 25, 2007. Three swaths for 0300 to 0600 UTC for the OMI data and covering the GEMS field of view were selected for analysis. Fig 2(a) and (b) show the ECF retrieved by OMI and GEMS, respectively. Fig. 2(c) shows the difference between the ECF retrieved by OMI and GEMS. Fig. 2(d) and (e) show the CCP retrieved by OMI and GEMS, respectively, while Fig. 2(f) shows the difference between the CCP retrieved by the two algorithms. The retrieved ECF had similar errors in each swath, with the errors most prominent in areas with a low ECF and the edge in RAA. These errors were strongly correlated (approximately 0.8) with RAA. Because GEMS is in a geostationary orbit, in which the discontinuous azimuth angle observed by polar-orbiting satellites such as OMI is reduced, consideration of RAA was minimized in the algorithm. This could be a major source of the differences between the two algorithms.

4.2 Comparison with TROPOMI Clouds

We evaluated the performance of the GEMS cloud retrieval algorithm using TROPOMI data, which can be collected simultaneously with GEMS data, taking into account orbital differences and the spectral ranges of observation. Similar to the experiments in Section 4.1, we conducted quantitative validation (Figure 4) and qualitative validation (Figure 4) for randomly selected days in March, June, September, and December 2021. Because TROPOMI cloud retrieval products are defined differently from GEMS products, we converted the CF provided by TROPOMI to an ECF using Equation (4) to represent the cloud amount and applied the CP for validation with the CCP. We performed cloud retrieval and analysis for three swaths (observation time 0300–0600 UTC) covering East Asia, which is the GEMS field of view. Figure 4 shows the results for March, June, September, and December from left to right, with the top panels showing the results for the ECF and the bottom panels showing the density scatterplot for the CCP. The x-axis in the top panel represents the converted CF values from TROPOMI to ECF, and the y-axis represents the ECF values obtained from GEMS using TROPOMI L1B radiance as input. The x-axis in the bottom panel for CCP represents the median values of CTP and CBP obtained from TROPOMI, and the y-axis represents

GEMS CCP using TROPOMI as input. There was no noticeable difference in the algorithm's performance for each season. However, for the ECF, because we corrected and compared the products with different definitions, we found that the linear relationship was not clear and the correlation coefficients were relatively low compared with the values in Figure 2.

Figure 5 shows the ECF (top) and CCP (bottom) obtained from TROPOMI (left) and GEMS (right) on September 16, 2021.

315 The difference in the ECF is pronounced in the Tibetan Plateau, and overall, there is a noticeable difference in the ECF between ocean and land areas. This is due to the fact that TROPOMI does not provide surface reflectance at 463 nm and instead uses surface reflectance at 420 nm as input data. As for the CCP, it is difficult to compare with the TROPOMI CP as the definitions differ, but overall, the GEMS CCP was lower in altitude than was the TROPOMI CP.

5 GEMS Cloud Retrieval Algorithm Results Using GEMS Radiances

320 The accuracy and usability of the cloud products retrieved by the GEMS cloud retrieval algorithm were evaluated by comparing them with products produced by other sensors and orbits, such as TROPOMI, AMI, and CALIOP, using data collected after an in-orbit test in 2021. Cases of high concentrations of fine dust, typhoons, and sea fog were selected to reflect the atmospheric environment and cloud characteristics over East Asia.

5.1 Air Pollution Case

325 As the main purpose of GEMS is to monitor air pollutants in East Asia, we selected a high-air-pollutant case. We analyzed the characteristics of clouds that appear during high concentrations of fine dust, as was the case in May 2021, Figures 5 and 6 show cloud detection and cloud pressure, respectively. The data analyzed were taken at approximately 0430 UTC, when the A-train satellite was passing over the region, and the 0445 UTC data were analyzed based on the GEMS field of view. Figure 5(a) shows the ECF result from GEMS, Figure 5(b) shows the ECF result from TROPOMI, Figure 5(c) shows the CF image

330 of AMI, and Figure 5(d) is an image of the aerosol optical depth (AOD) derived from AMI.

Comparing GEMS and AMI clouds, it is clear that AMI identifies many more areas as clouds compared with GEMS as it was designed to observe meteorological phenomena, and is particularly sensitive to clouds. The TROPOMI and GEMS cloud fractions in Fig. 5(c) appear almost similar in shape, confirming that the two instruments detect clouds at a similar degree of sensitivity. The GEMS cloud retrieval algorithm uses surface reflectance climatology from OMI as input, making it possible

335 to expose the surface properties in the ECF as the surface reflectance data is not updated. In Fig. 5(d), which represents the AMI AOD, a high-concentration fine-dust belt in the southern region of the Korean Peninsula is clearly visible. GEMS and TROPOMI both detected a thin cloud (ECF < 0.2) in this region. As the cloud-production algorithms of GEMS and TROPOMI do not provide additional information on aerosols, it was difficult to classify aerosols from cloud data, indicating a shortcoming of the GEMS cloud retrieval algorithm.

340 Fig. 6 shows the CCP validation result for the same day as Fig. 5. Fig. 6(a) displays the GEMS CCP, while Fig. 6(b) shows the TROPOMI mCP. Fig. 6(c) shows the CTP provided by AMI, and Fig. 6(d) is an image overlaying the cloud products of

three satellites on the CALIOP VFM. In Fig. 6(d), black dots represent GEMS CCP, blue dots represent AMI CTP, gray shading represents the range between TROPOMI CTP and CBP, pink shading represents the region where clouds were detected by CALIOP VFM, and orange shading represents the region where aerosols were detected. To compare with CALIOP VFM, the CCP analysis figures, such as Fig. 6, use height units. In Equation (4) the units have been converted to height.

The cloud height results displayed in Figure 6(a)–(c) exhibit distinctive characteristics for each satellite, making it difficult to find commonalities. GEMS values were similar to surface height for clear pixels, while for areas with aerosols, the retrieved CH values were within the range associated with aerosols. The algorithm used by GEMS cannot distinguish between clouds and aerosols, and the scattering effect at the wavelengths used for cloud retrieval causes the cloud altitude to be calculated as if there were clouds instead of the aerosols that are actually present due to the reflection effect caused by aerosols. Comparing TROPOMI CH with GEMS CH revealed that, in general, GEMS tends to concur with TROPOMI CH in low cloud (less than 6 km) conditions, but estimates lower cloud heights than TROPOMI cloud pressure calculations for high cloud (over 6 km). The scale pressure of O_2-O_2 absorption is approximately 700 hPa, and this altitude becomes the reference for the relationship between TROPOMI and GEMS cloud pressure. Consequently, while lower clouds display cloud heights comparable to TROPOMI, clouds at higher altitudes have the characteristic of estimating lower altitudes.

Due to the GEO orbit in which the GEMS is located, there are temporal variations in SZA as well as several input variables. Using the time-specific (04:45 UTC) observation data of the air pollution case, we tested the error when input variables over time were not taken into account and were inaccurately entered as fixed values. The results indicate that the largest error in cloud calculation occurs when the SZA change is not adequately accounted for. The surface reflection, which causes an approximately 1% change in time, also caused a significant error, and the error characteristics in the land-ocean were found to be substantially different. The error caused by a minor change in ground pressure over time was insignificant.

5.2 Typhoon Case

Typhoons are meteorological phenomena that involve wide variety of clouds, making them a useful case for cloud verification. Typhoon Chantu, which occurred in September 2021, was a large typhoon to the southwest of the Korean Peninsula, as can be seen in Fig. 7(a)–(c). Figure 7 also contains the results of each satellite's cloud detection, as in Figure 5, but excludes verification of AOD because we focused on clouds. As a well-developed tropical low-pressure system, a typhoon is accompanied by various types of clouds, ranging from thick clouds to cirrus formations, providing insight into how GEMS retrieves different types of clouds. In Fig. 7(a), the ECF is significantly high around the eye of the typhoon. TROPOMI and AMI also showed high agreement in cloud detection for thick clouds.

The clouds that come with typhoons are useful for understanding the general characteristics of cloud distribution. However, if the clouds are sufficiently thick, the active sensor on CALIOP has limited penetration and may not provide enough information about what lies beneath the clouds. Comparing cloud height from Fig. 7(a) to (c), GEMS cloud height is lower than the heights estimated by other satellites in general. We therefore analyzed the vertical structure of the clouds for details using Figure 8(d), in which the VFM of typhoon clouds being reported only in the upper atmosphere can be attributed to the thick clouds. AMI,

375 which produced the cloud-top height in Fig. 7(d), reports clouded at high altitudes similar to those reported by CALIOP VFM, except for the typhoon eye. Cloud height produced by GEMS and TROPOMI also accurately detected the typhoon eye, and, as shown in Fig. 6, GEMS tended to underestimate cloud height compared with TROPOMI in high and thick cloud conditions. In addition, while AMI produced CTH in the upper atmosphere for areas estimated to be multi-layered above 40° latitude, the GEMS CCP tended to produce cloud height in the lower layer. These characteristics can be useful for understanding the

380 properties of multi-layered clouds in further studies.

Analysis of cloud production characteristics over time is required despite the fact that verification with other satellites is not feasible for all GEMS observation times except when some paths overlap. In the case of typhoons in which clouds are transparent and move rapidly over time, the observation of cloud movement over time was therefore qualitatively analyzed. It was discovered that GEMS cloud retrieval algorithm accurately identified the movement of typhoons over time.

385 **5.3 Sea Fog Case**

Sea fog is a common on the western coast of Korea and can be included in the transport path of air pollutants. False detection of sea fog can lead to significant errors in observations of atmospheric pollutants using GEMS. In Figure 9, sea fog is difficult to distinguish from low-level clouds over the ocean using only the naked eye, but it can be identified by observing its movement over time from a geostationary orbit. Unlike clouds, sea fog tends to linger near the coast and has little flow. All three cloud

390 fractions, GEMS, TROPOMI, and AMI, mistook the presence of sea fog as evidence of clouds.

As sea fog induces high reflectance, accurate retrieval of CCP is essential for correcting atmospheric pollutant observations. In the case of GEMS, sea level pressure can be obtained for areas suspected of being susceptible to sea fog, and it is useful for correcting the influence of sea fog on atmospheric components retrievals. TROPOMI, which uses the near-infrared region for cloud retrieval, also retrieves CP in sea fog–prone areas close to the surface altitude, and AMI shows a tendency to retrieve

395 cloud heights similar to those of low-level clouds. If the cloud height in GEMS is overestimated, as in the case of AMI, it may overestimate atmospheric components.

6 Conclusions and Discussions

In this study, we introduced, compared, and validated the GEMS cloud retrieval algorithm and its products. The GEMS cloud retrieval algorithm is based on an algorithm developed for the polar-orbiting OMI satellite, and therefore produces values

400 similar to OMI's cloud products. with a correlation coefficient greater than 0.94 for all seasons. Although it was difficult to make quantitative comparisons due to different definitions of clouds, we also validated GEMS data using data from TROPOMI, a UV-Vis environmental satellite currently in operation. The ECF was comparable to TROPOMI in general. Also, compared to TROPOMI CP, the CCP was overestimated at pressures lower than scale pressure and underestimated at pressures over than scale pressure. It demonstrates its suitability for use in trace-gas corrections.

405 As GEMS operates in a geostationary orbit, unlike previous environmental satellites, it is important to detect diurnal cloud characteristics that appear over East Asia. In this study, cases of air pollutants, typhoons, and sea fog, all of which are common in East Asia, were selected to compare and verify the GEMS cloud data with those of other satellites. Cloud heights produced by GEMS, TROPOMI, and AMI were compared based on a CALIOP VFM, which can observe the vertical distribution of clouds. CALIOP was found to be insufficient for detecting thick, low-altitude clouds. The GEMS cloud retrieval algorithm is

410 sensitive to high pressure greater than scale pressure; as a result, GEMS estimates of cloud height were the lowest among the four satellites, corresponding to the height at which clouds reflect radiation. The cloud-top height produced by TROPOMI was located at a lower altitude compared with the AMI CTH, and GEMS CH was usually following TROPOMI CH. AMI generally produced cloud-top heights that closely matched the top of CALIOP VFM, but tended to overestimate cloud height in the case of sea fog. Through comparisons of GEMS ECF and CCP, we confirmed that the cloud characteristics were well reflected in

415 the retrieval results, and it is expected to be useful for correcting the beam path length of observed radiation.

The current version of the GEMS cloud retrieval algorithm generates results consistent with the output produced by other satellites and appears to accurately reflect cloud characteristics in East Asia. However, two issues have been pointed out. First, the reflectivity and pressure characteristics of inland regions, including the Tibetan Plateau, are directly reflected in the derived ECF, and (2) the ECF was greater than zero in most regions. This is due to the current algorithm using OMI climatological

420 data as input values for surface reflectance. The surface reflectance from OMI is difficult to represent due to the influence of changes in background aerosols in the atmosphere, among other factors (M. Kim et al., 2021). In the next version of the algorithm update, we plan to replace the input value with surface reflectance observed by GEMS, which is expected to address both problems. Since the GEMS cloud is retrieved through the DOAS method using linear fitting, it is necessary to compare the results with nonlinear fitting. One approach for applying nonlinear fitting is to utilize QDOAS, as demonstrated by

425 Danckaert et al. (2012). We plan to analyze the results of cloud retrievals using the nonlinear fitting method in existing algorithm in future research. Also, QDOAS application enable to consider the NO_2 absorption. We anticipate the improvement of the GEMS cloud retrieval algorithm in the future through consider those remaining issues.

Funding

This subject is supported by Korea Ministry of Environment (MOE) as Public Technology Program based on Environmental
430 Policy (2017000160003).

References

Acarreta, J., De Haan, J., and Stammes, P.: Cloud pressure retrieval using the O_2-O_2 absorption band at 477 nm, Journal of Geophysical Research: Atmospheres, 109, 2004.

Baek, K., Kim, J. H., Bak, J., Haffner, D. P., Kang, M., and Hong, H.: Evaluation of total ozone measurements from
435 Geostationary Environmental Monitoring Satellite (GEMS), EGUsphere, 1-23, 2022.

Bak, J., Baek, K.-H., Kim, J.-H., Liu, X., Kim, J., and Chance, K.: Cross-evaluation of GEMS tropospheric ozone retrieval
performance using OMI data and the use of an ozonesonde dataset over East Asia for validation, Atmospheric Measurement
Techniques, 12, 5201-5215, 2019.

Bovensmann, H., Burrows, J., Buchwitz, M., Frerick, J., Noel, S., Rozanov, V., Chance, K., and Goede, A.: SCIAMACHY:
440 Mission objectives and measurement modes, Journal of the atmospheric sciences, 56, 127-150, 1999.

Brion, J., Chakir, A., Charbonnier, J., Daumont, D., Parisse, C., and Malicet, J.: Absorption spectra measurements for the
ozone molecule in the 350–830 nm region, Journal of atmospheric chemistry, 30, 291-299, 1998.

Burrows, J. P., Weber, M., Buchwitz, M., Rozanov, V., Ladstätter-Weißenmayer, A., Richter, A., DeBeek, R., Hoogen, R.,
Bramstedt, K., and Eichmann, K.-U.: The global ozone monitoring experiment (GOME): Mission concept and first scientific
445 results, Journal of the Atmospheric Sciences, 56, 151-175, 1999.

Chimot, J., Veefkind, J. P., Vlemmix, T., and Levelt, P. F.: Spatial distribution analysis of the OMI aerosol layer height: a
pixel-by-pixel comparison to CALIOP observations, Atmospheric Measurement Techniques, 11, 2257-2277, 2018.

Choi, W., Lee, H., Kim, J., and Park, J.: First TROPOMI Retrieval of Aerosol Effective Height Using O_4 Absorption Band at
477 nm and Aerosol Classification, IEEE Transactions on Geoscience and Remote Sensing, 59, 9873-9886, 2020.

450 Compernolle, S., Argyrouli, A., Lutz, R., Sneep, M., Lambert, J.-C., Fjæraa, A. M., Hubert, D., Keppens, A., Loyola, D., and
O'Connor, E.: Validation of the Sentinel-5 Precursor TROPOMI Cloud Data with Cloudnet, Aura OMI O_2–O_2, MODIS, and
Suomi-NPP VIIRS, Atmospheric Measurement Techniques, 14, 2451-2476, 2021.

Danckaert, T., Fayt, C., Van Roozendael, M., De Smedt, I., Letocart, V., Merlaud, A., and Pinardi, G.: QDOAS Software user
manual, 2012.

455 Flynn, C. M., Pickering, K. E., Crawford, J. H., Lamsal, L., Krotkov, N., Herman, J., Weinheimer, A., Chen, G., Liu, X., and
Szykman, J.: Relationship between column-density and surface mixing ratio: Statistical analysis of O_3 and NO_2 data from the
July 2011 Maryland DISCOVER-AQ mission, Atmospheric Environment, 92, 429-441, 2014.

Frankenberg, C., Pollock, R., Lee, R., Rosenberg, R., Blavier, J.-F., Crisp, D., O'Dell, C., Osterman, G., Roehl, C., and
Wennberg, P.: The Orbiting Carbon Observatory (OCO-2): spectrometer performance evaluation using pre-launch direct sun
460 measurements, Atmospheric Measurement Techniques, 8, 301-313, 2015.

Go, S., Kim, J., Park, S. S., Kim, M., Lim, H., Kim, J.-Y., Lee, D.-W., and Im, J.: Synergistic use of hyperspectral uv-visible
omi and broadband meteorological imager modis data for a merged aerosol product, Remote Sensing, 12, 3987, 2020.

Hong, H., Lee, H., Kim, J., Jeong, U., Ryu, J., and Lee, D. S.: Investigation of simultaneous effects of aerosol properties and
aerosol peak height on the air mass factors for space-borne NO2 retrievals, Remote Sensing, 9, 208, 2017.

465 Hsu, N. C., McPeters, R. D., Seftor, C. J., and Thompson, A. M.: Effect of an improved cloud climatology on the total ozone
mapping spectrometer total ozone retrieval, Journal of Geophysical Research: Atmospheres, 102, 4247-4255, 1997.

Jervis, D., McKeever, J., Durak, B. O., Sloan, J. J., Gains, D., Varon, D. J., Ramier, A., Strupler, M., and Tarrant, E.: The GHGSat-D imaging spectrometer, Atmospheric Measurement Techniques, 14, 2127-2140, 2021.

Joiner, J. and Vasilkov, A. P.: First results from the OMI rotational Raman scattering cloud pressure algorithm, IEEE transactions on geoscience and remote sensing, 44, 1272-1282, 2006.

Joiner, J., Vasilkov, A., Gupta, P., Bhartia, P., Veefkind, P., Sneep, M., de Haan, J., Polonsky, I., and Spurr, R.: Fast simulators for satellite cloud optical centroid pressure retrievals; evaluation of OMI cloud retrievals, Atmospheric Measurement Techniques, 5, 529-545, 2012.

Kang, M., Ahn, M.-H., Liu, X., Jeong, U., and Kim, J.: Spectral calibration algorithm for the geostationary environment monitoring spectrometer (GEMS), Remote Sensing, 12, 2846, 2020.

Kim, H.-S., Baum, B. A., and Choi, Y.-S.: Use of spectral cloud emissivities and their related uncertainties to infer ice cloud boundaries: methodology and assessment using CALIPSO cloud products, Atmospheric Measurement Techniques, 12, 5039-5054, 2019.

Kim, G., Choi, Y.-S., Park, S. S., and Kim, J.: Effect of solar zenith angle on satellite cloud retrievals based on O_2–O_2 absorption band, International Journal of Remote Sensing, 42, 4224-4240, 2021.

Kim, M., Kim, S. H., Kim, W. V., Lee, Y. G., Kim, J., and Kafatos, M. C.: Assessment of Aerosol optical depth under background and polluted conditions using AERONET and VIIRS datasets, Atmospheric Environment, 245, 117994, 2021.

Kim, J., Jeong, U., Ahn, M.-H., Kim, J. H., Park, R. J., Lee, H., Song, C. H., Choi, Y.-S., Lee, K.-H., and Yoo, J.-M., et al.: New era of air quality monitoring from space: Geostationary Environment Monitoring Spectrometer (GEMS), Bulletin of the American Meteorological Society, 101, E1-E22, 2020.

Kim, M., Kim, J., Torres, O., Ahn, C., Kim, W., Jeong, U., Go, S., Liu, X., Moon, K. J., and Kim, D.-R.: Optimal estimation-based algorithm to retrieve aerosol optical properties for GEMS measurements over Asia, Remote Sensing, 10, 162, 2018.

Kleipool, Q., Dobber, M., de Haan, J., and Levelt, P.: Earth surface reflectance climatology from 3 years of OMI data, Journal of Geophysical Research: Atmospheres, 113, 2008.

Kwon, H.-A., Park, R. J., Jeong, J. I., Lee, S., González Abad, G., Kurosu, T. P., Palmer, P. I., and Chance, K.: Sensitivity of formaldehyde (HCHO) column measurements from a geostationary satellite to temporal variation of the air mass factor in East Asia, Atmospheric Chemistry and Physics, 17, 4673-4686, 2017.

Latsch, M., Richter, A., Eskes, H., Sneep, M., Wang, P., Veefkind, P., Lutz, R., Loyola, D., Argyrouli, A., Valks, P., Wagner, T., Sihler, H., van Roozendael, M., Theys, N., Yu, H., Siddans, R., and Burrows, J. P.: Intercomparison of Sentinel-5P TROPOMI cloud products for tropospheric trace gas retrievals, Atmospheric Measurement Techniques, 15, 6257–6283, 2022.

Lee, Y., Ahn, M.-H., and Kang, M.: The new potential of deep convective clouds as a calibration target for a geostationary UV/VIS hyperspectral spectrometer, Remote Sensing, 12, 446, 2020.

Lee, Y., Ahn, M. H., Kang, M., & Eo, M.: Spectral replacement using machine learning methods for continuous mapping of the Geostationary Environment Monitoring Spectrometer (GEMS). Atmospheric Measurement Techniques, 16(1), 153-168, 2023.

Levelt, P. F., Van Den Oord, G. H., Dobber, M. R., Malkki, A., Visser, H., De Vries, J., Stammes, P., Lundell, J. O., and Saari, H.: The ozone monitoring instrument, IEEE Transactions on geoscience and remote sensing, 44, 1093-1101, 2006.

Loyola, D. G., Gimeno García, S., Lutz, R., Argyrouli, A., Romahn, F., Spurr, R. J., Pedergnana, M., Doicu, A., Molina García, V., and Schüssler, O.: The operational cloud retrieval algorithms from TROPOMI on board Sentinel-5 Precursor, Atmospheric

505   Measurement Techniques, 11, 409-427, 2018.

Miller, S. D., Mills, S. P., Elvidge, C. D., Lindsey, D. T., Lee, T. F., and Hawkins, J. D.: Suomi satellite brings to light a unique frontier of nighttime environmental sensing capabilities, Proceedings of the National Academy of Sciences, 109, 15706-15711, 2012.

Park, S. S., Kim, S.-W., Song, C.-K., Park, J.-U., and Bae, K.-H.: Spatio-temporal variability of aerosol optical depth, total

510   ozone and NO_2 over East Asia: Strategy for the validation to the GEMS Scientific Products, Remote Sensing, 12, 2256, 2020.

Park, J., Choi, W., Lee, H.-M., Park, R. J., Kim, S.-Y., Yu, J.-A., Lee, D.-W., and Lee, H.: Effect of Error in SO2 Slant Column Density on the Accuracy of SO_2 Transport Flow Rate Estimates Based on GEMS Synthetic Radiances, Remote Sensing, 13, 3047, 2021.

Platt, U., Perner, D., and Pätz, H.: Simultaneous measurement of atmospheric CH_2O, O_3, and NO_2 by differential optical

515   absorption, Journal of Geophysical Research: Oceans, 84, 6329-6335, 1979.

Sneep, M., De Haan, J., Stammes, P., Wang, P., Vanbauce, C., Joiner, J., Vasilkov, A., and Levelt, P.: Three-way comparison between OMI and PARASOL cloud pressure products, Journal of Geophysical Research: Atmospheres, 113, 2008.

Spurr, R. J.: VLIDORT: A linearized pseudo-spherical vector discrete ordinate radiative transfer code for forward model and retrieval studies in multilayer multiple scattering media, Journal of Quantitative Spectroscopy and Radiative Transfer, 102,

520   316-342, 2006.

Stammes, P., Sneep, M., De Haan, J., Veefkind, J., Wang, P., and Levelt, P.: Effective cloud fractions from the Ozone Monitoring Instrument: Theoretical framework and validation, Journal of Geophysical Research: Atmospheres, 113, 2008.

Taylor, T. E., O'Dell, C. W., O'Brien, D. M., Kikuchi, N., Yokota, T., Nakajima, T. Y., Ishida, H., Crisp, D., and Nakajima, T.: Comparison of cloud-screening methods applied to GOSAT near-infrared spectra, IEEE Transactions on Geoscience and

525   Remote Sensing, 50, 295-309, 2011.

Thalman, R. and Volkamer, R.: Temperature dependent absorption cross-sections of O_2–O_2 collision pairs between 340 and 630 nm and at atmospherically relevant pressure, Physical chemistry chemical physics, 15, 15371-15381, 2013.

Vandaele, A. C., Lopez-Moreno, J. J., Patel, M. R., Bellucci, G., Daerden, F., Ristic, B., ... & NOMAD Team.: NOMAD, an integrated suite of three spectrometers for the ExoMars trace gas mission: Technical description, science objectives and

530   expected performance. Space Science Reviews, 214, 1-47, 2018.

Vasilkov, A., Joiner, J., Spurr, R., Bhartia, P. K., Levelt, P., and Stephens, G.: Evaluation of the OMI cloud pressures derived from rotational Raman scattering by comparisons with other satellite data and radiative transfer simulations, Journal of Geophysical Research: Atmospheres, 113, 2008.

Vasilkov, A., Yang, E.-S., Marchenko, S., Qin, W., Lamsal, L., Joiner, J., Krotkov, N., Haffner, D., Bhartia, P. K., and Spurr,

535   R.: A cloud algorithm based on the O_2-O_2 477 nm absorption band featuring an advanced spectral fitting method and the use of surface geometry-dependent Lambertian-equivalent reflectivity, Atmospheric Measurement Techniques, 11, 4093-4107, 2018.

Veefkind, J. P., De Haan, J. F., Sneep, M., and Levelt, P. F.: Improvements to the OMI O_2–O_2 operational cloud algorithm and comparisons with ground-based radar–lidar observations, Atmospheric Measurement Techniques, 9, 6035-6049, 2016.

540   Veefkind, J. P., Aben, I., McMullan, K., Förster, H., De Vries, J., Otter, G., Claas, J., Eskes, H., De Haan, J., and Kleipool, Q.: TROPOMI on the ESA Sentinel-5 Precursor: A GMES mission for global observations of the atmospheric composition for climate, air quality and ozone layer applications, Remote sensing of environment, 120, 70-83, 2012.

Wang, P. and Stammes, P.: Evaluation of SCIAMACHY Oxygen A band cloud heights using Cloudnet measurements, Atmospheric Measurement Techniques, 7, 1331-1350, 2014.

545   Wang, P., Stammes, P., Van Der A, R., Pinardi, G., and Van Roozendael, M.: FRESCO+: an improved O_2 A-band cloud retrieval algorithm for tropospheric trace gas retrievals, Atmospheric Chemistry and Physics, 8, 6565-6576, 2008.

Wang, S., Liu, C., Zhang, W., Hao, N., Gimeno García, S., Xing, C., Zhang, C., Su, W., and Liu, J.: Development and Application of HECORA Cloud Retrieval Algorithm Based On the O_2-O_2 477 nm Absorption Band, Remote Sensing, 12, 3039, 2020.

550   Winker, D. M., Vaughan, M. A., Omar, A., Hu, Y., Powell, K. A., Liu, Z., Hunt, W. H., and Young, S. A.: Overview of the CALIPSO mission and CALIOP data processing algorithms, Journal of Atmospheric and Oceanic Technology, 26, 2310-2323, 2009.

Yang, J., Li, S., Gong, W., Min, Q., Mao, F., and Pan, Z.: A fast cloud geometrical thickness retrieval algorithm for single-layer marine liquid clouds using OCO-2 oxygen A-band measurements, Remote Sensing of Environment, 256, 112305, 2021.

555   Yoshida, Y., Ota, Y., Eguchi, N., Kikuchi, N., Nobuta, K., Tran, H., Morino, I., and Yokota, T.: Retrieval algorithm for CO_2 and CH_4 column abundances from short-wavelength infrared spectral observations by the Greenhouse gases observing satellite, Atmospheric Measurement Techniques, 4, 717-734, 2011.

Table 1: Values of each nodal point used to calculate the look-up table in the GEMS cloud retrieval algorithm.

Parameters	Values
Solar zenith angle (°)	0, 18.2, 25.8, 31.8, 36.9, 41.4, 45.6, 49.5, 53.1, 56.6, 60.0, 63.3, 66.4, 69.5, 72.5, 75.5, 78.5, 81.4, 84.3
Viewing zenith angle (°)	0, 18.2, 25.8, 31.8, 36.9, 41.4, 45.6, 49.5, 53.1, 56.6, 60.0, 63.3, 66.4, 69.5, 72.5, 75.5, 78.5, 81.4, 84.3
Relative azimuth angle (°)	0, 90, 180
Surface pressure (hPa)	1014, 1000, 950, 900, 850, 800, 750, 700, 600, 500, 400, 300, 200, 100

Surface reflectance	0, 0.05, 0.1, 0.2, 0.3, 0.4, 0.5, 0.6, 0.7, 0.8, 0.9, 1.0
Effective cloud pressure	0, 0.05, 0.1, 0.15, 0.2, 0.25, 0.3, 0.35, 0.4, 0.45, 0.5, 0.55, 0.6, 0.65, 0.7, 0.75, 0.8, 0.85, 0.9, 0.95, 1.0
Cloud centroid pressure (hPa)	1014, 1000, 950, 900, 850, 800, 750, 700, 600, 500, 400, 300, 200, 100

560

Table 2: Overview of the cloud products included in this study.

Instruments	Cloud product name	Variable	Spectral range (nm)
OMI	OMCLDO2	Effective cloud fraction Cloud height	470–490
TROPOMI	ROCINN CRB	Cloud fraction Cloud albedo Cloud pressure/height	758–766
GEMS	GEMS CLD	Effective cloud fraction Cloud centroid pressure	470–485
AMI	GK2A CTH	Cloud top height	412–12300
CALIOP	VFM	Vertical feature mask	532, 1064
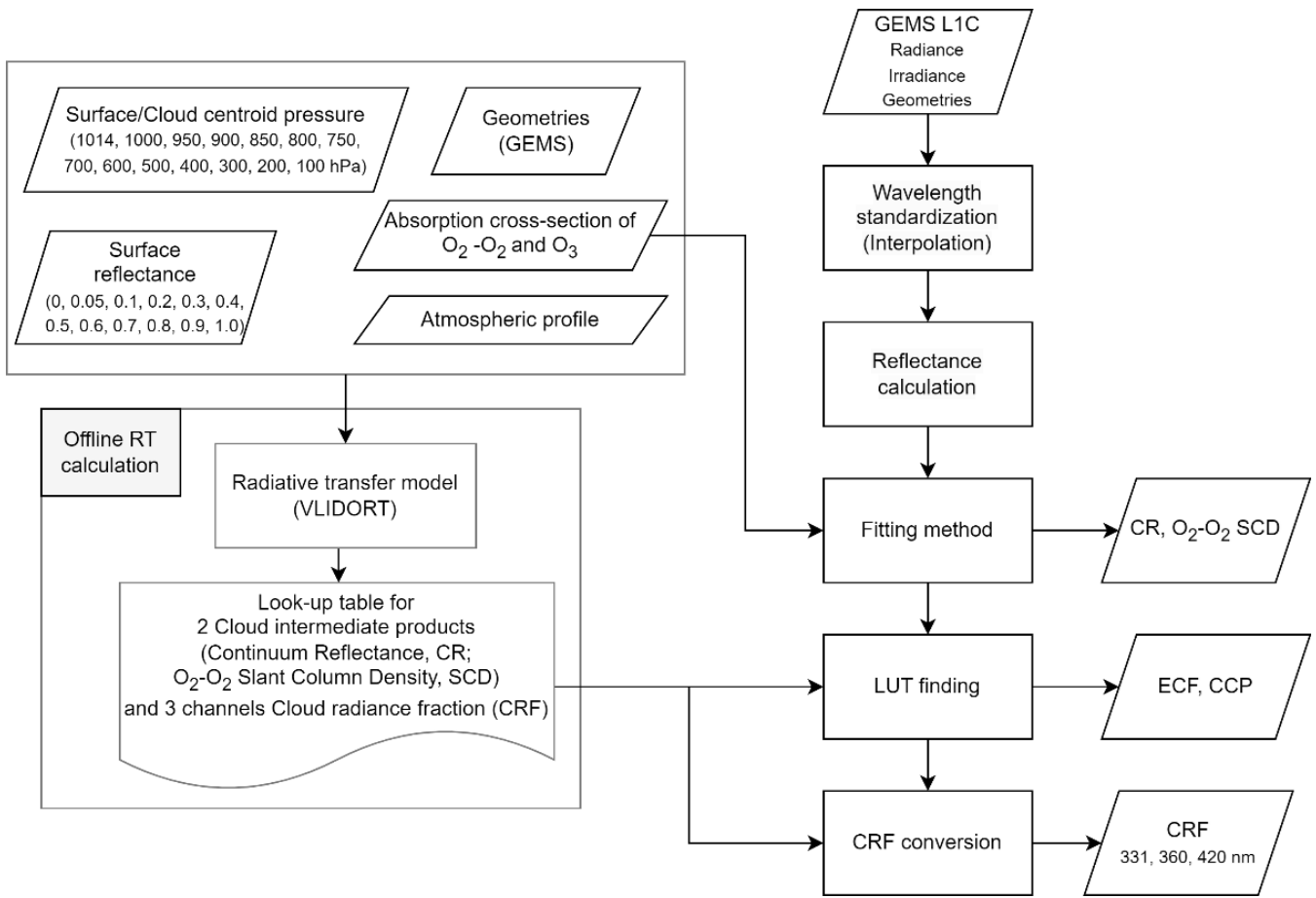
Figure 1: GEMS cloud retrieval algorithm flowchart.

565
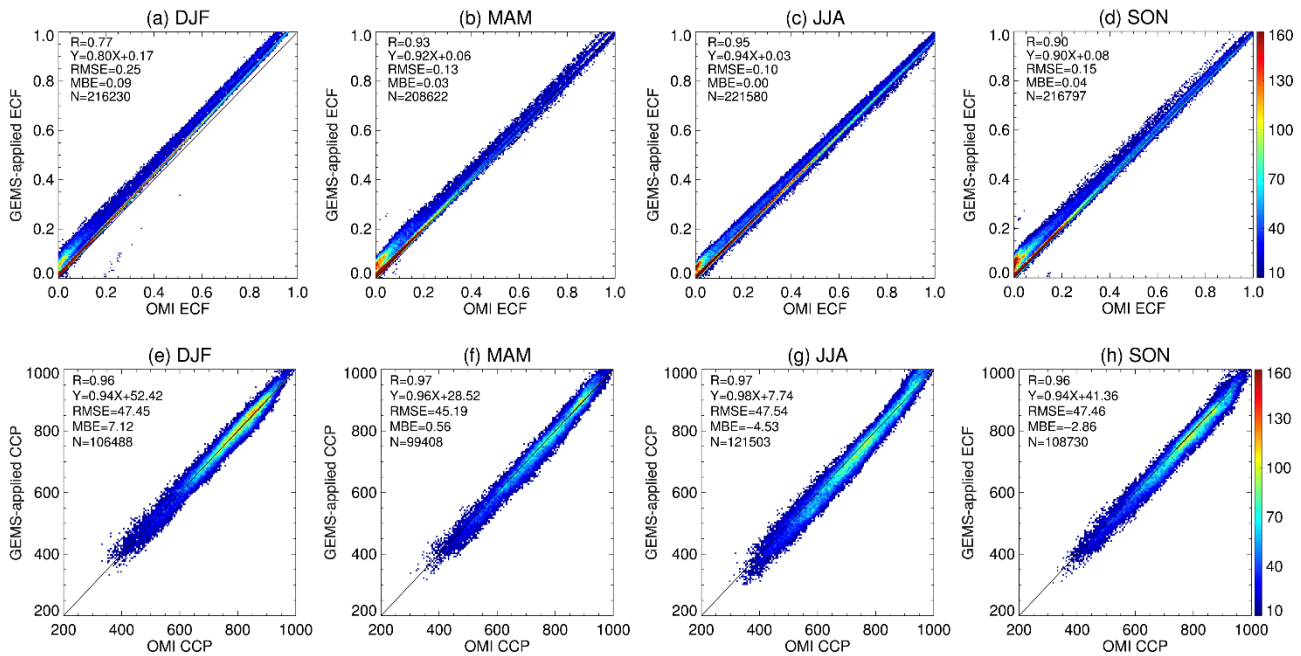
Figure 2: Cloud products for random days in each month of 2007 (classified by seasons: DJF-winter, MAM-spring, JJA-summer, SON-autumn) for comparison with cloud products from the OMI algorithm. The top panel shows the density scatterplot for effective cloud fraction (ECF) and the bottom panel shows the density scatter plot for cloud centroid pressure (CCP). The x-axis represents the values from OMI, and the y-axis represents the cloud products from the GEMS algorithm. The solid line indicates the 1:1 line, and the correlation coefficient (R), regression equation, root mean square error (RMSE), mean bias error (MBE), and number of pixels (#) used in the analysis are presented.
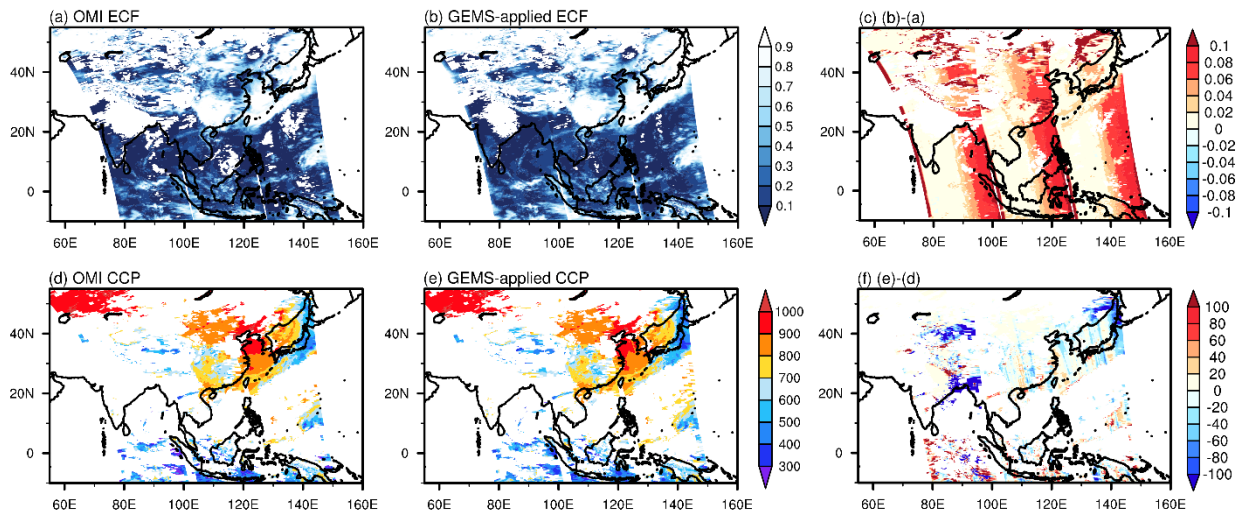
Figure 3: Results of performance validation of the GEMS cloud retrieval algorithm using OMI data. The data from March 25, 2007, were used as input. (a) ECF provided by OMI. (b) ECF retrieved by GEMS using OMI L1B data. (d) CCP retrieved by OMI. (e) CCP image retrieved by GEMS using the OMI radiance data input same as (b). (c) and (f) Differences in cloud retrieval between the GEMS and OMI algorithms.
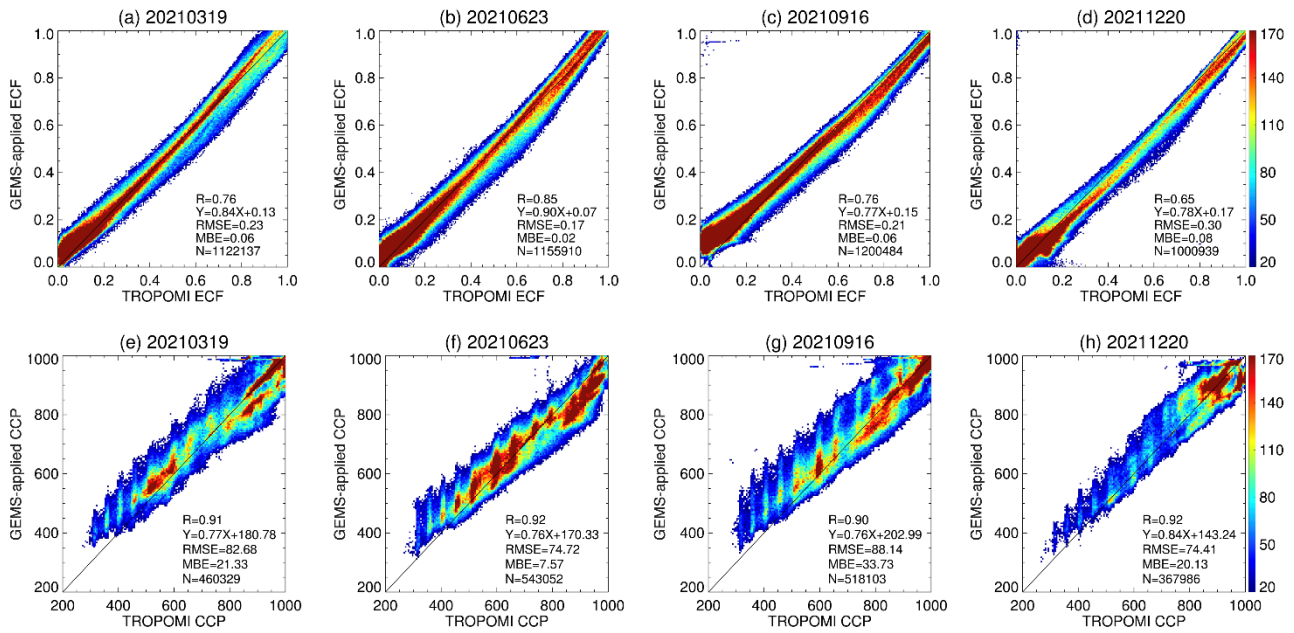
Figure 4: This figure is similar to Figure 1 but for TROPOMI. To verify the performance and seasonal dependency of GEMS cloud retrieval algorithm, cloud retrieval results were compared with those of TROPOMI for random days in March, May, September, and December 2021. The top panel shows the results for ECF and the bottom panel shows the results for CCP in a density scatterplot. As definitions of cloud pressure differ between GEMS and TROPOMI, the density scatterplot was generated using the mean value of CTP and CBP (mean cloud pressure, mCP) from TROPOMI. The x-axis shows the TROPOMI values, and the y-axis shows the GEMS cloud retrieval results. The solid line represents the 1:1 line, and the correlation coefficient and regression equation are also displayed.
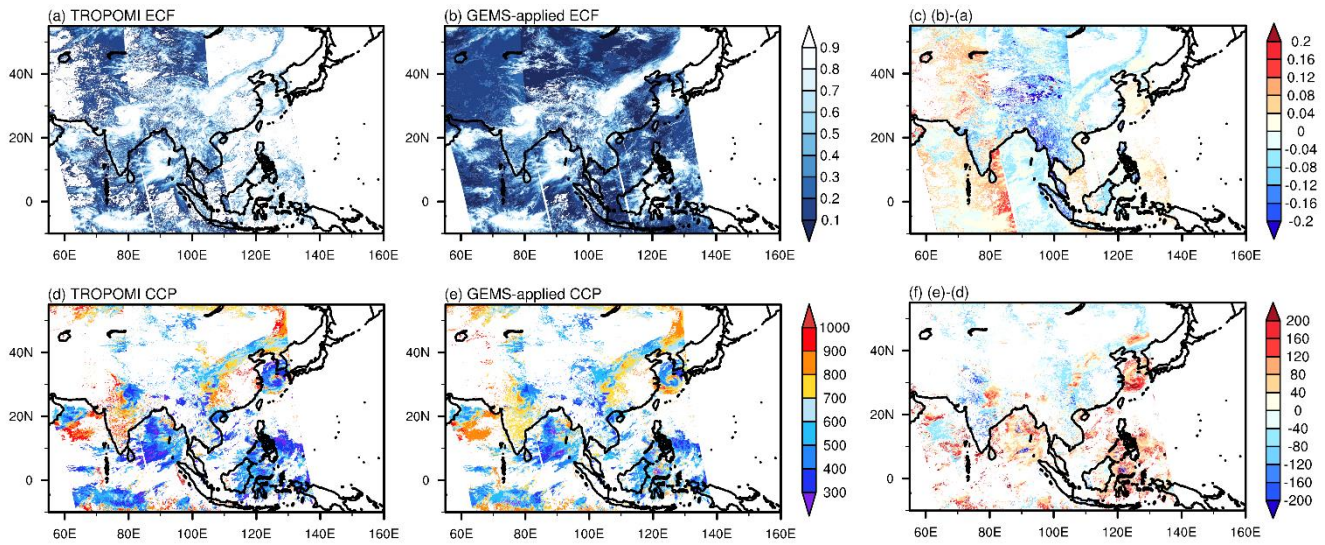
Figure 5: This figure, similar to Figure 2, shows the validation of the GEMS cloud retrieval algorithm using TROPOMI data. Cloud retrievals were performed using observations from September 16, 2021, as input. (a) TROPOMI CF converted to ECF. (b) ECF derived from GEMS using TROPOMI L1B as input. (d) CP retrieved from TROPOMI. (e) CCP image retrieved by GEMS cloud retrieval algorithm. (c) and (f) Differences in cloud retrievals between GEMS and TROPOMI algorithms.
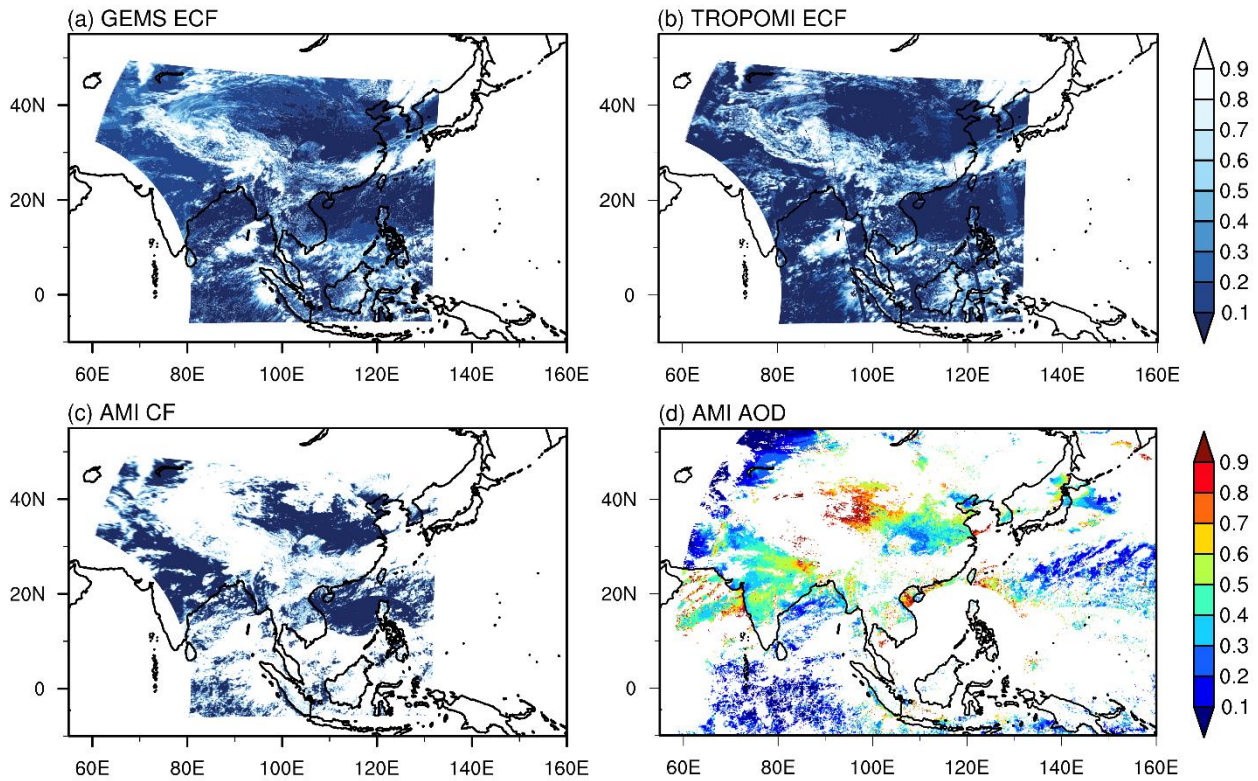
Figure 6: Four different images of air pollutants as observed on May 8, 2021, in the GEMS field of view. (a) ECF retrieved by GEMS. (b) ECF calculated by converting the CF data from TROPOMI. (c) CF image calculated by collocating AMI data to GEMS pixels.
595 **(d) Aerosol optical depth (AOD) image obtained from AMI data.**
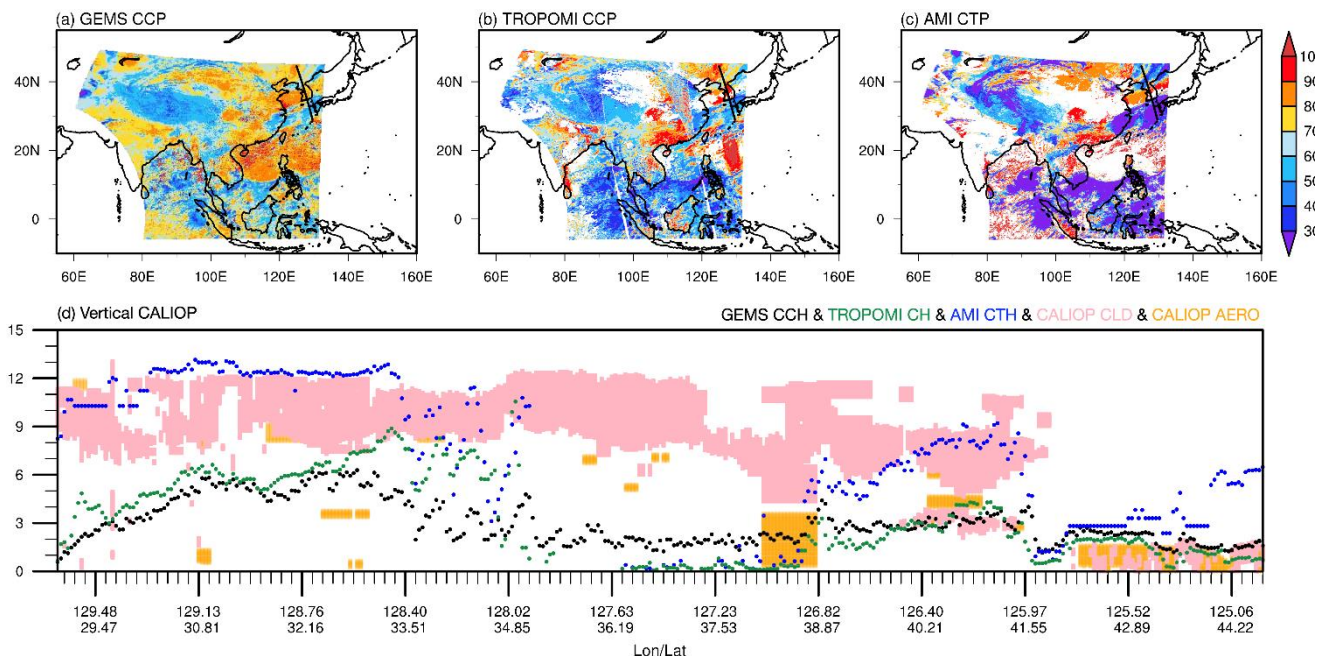
Figure 7: Cloud pressure observations on May 8, 2021. (a) GEMS CCP. (b) TROPOMI mCP. (c) AMI CTP. (d) CALIOP VFM with cloud pressure products. In (a) to (c), the thick black line represents the scan path of CALIOP. In (d), a black dot represents GEMS CCP, a blue dot represents GK2A CTP, the gray shade represents between the TROPOMI CTP and CBP, the pink shade represents a CALIOP cloud mask, and the orange shade represents a CALIOP aerosol mask.
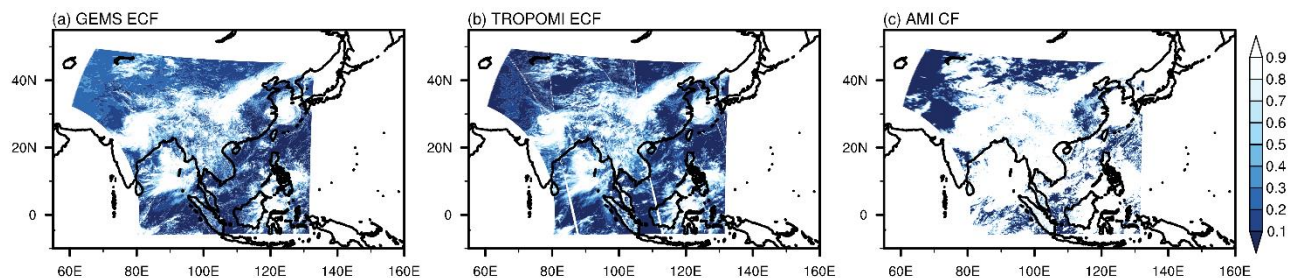
Figure 8: Similar to Figure 5, an intercomparison of ECF is presented for the case of Typhoon Chantu, which occurred on September 16, 2021. (a) GEMS ECF. (b) TROPOMI ECF. (c) AMI CF.
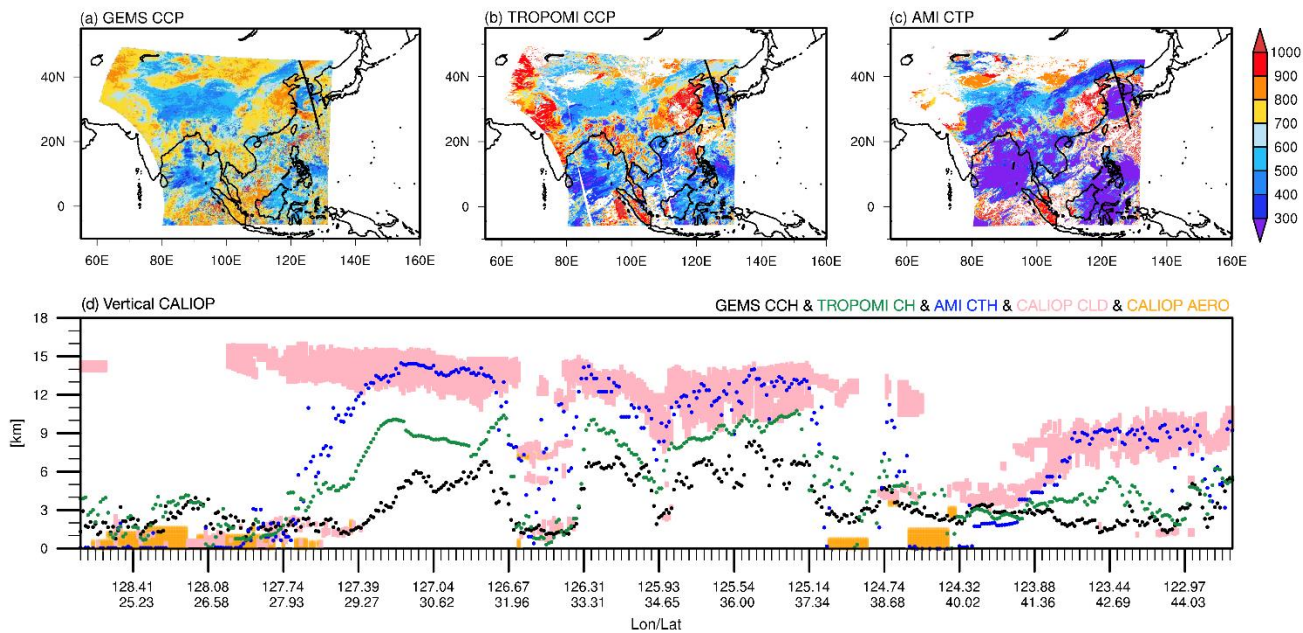
Figure 9: The case of Typhoon Chantu on September 16, 2021. (a) CCP obtained from GEMS. (b) mCP from TROPOMI. (c) CTP derived from AMI. (d) CHs converted to cloud altitude from three satellites overlaid on the CALIOP VFM image.
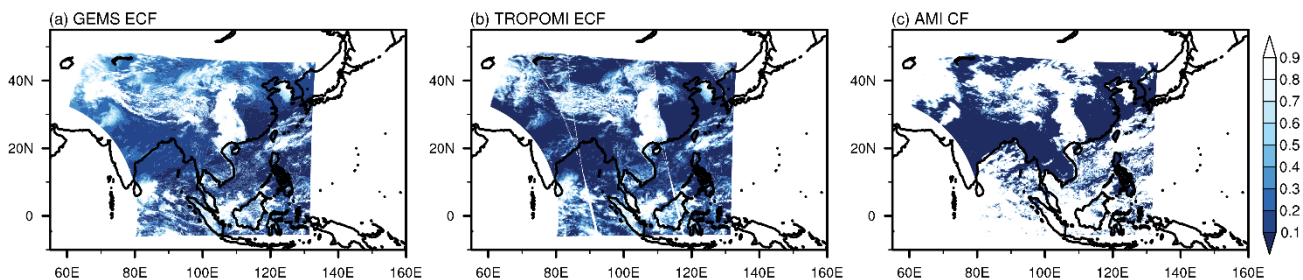
Figure 10: Similar to Figure 7, intercomparison of ECF for the case of sea fog, which occurred on March 25, 2021. (a) GEMS ECF. (b) TROPOMI ECF. (c) AMI CF.

610
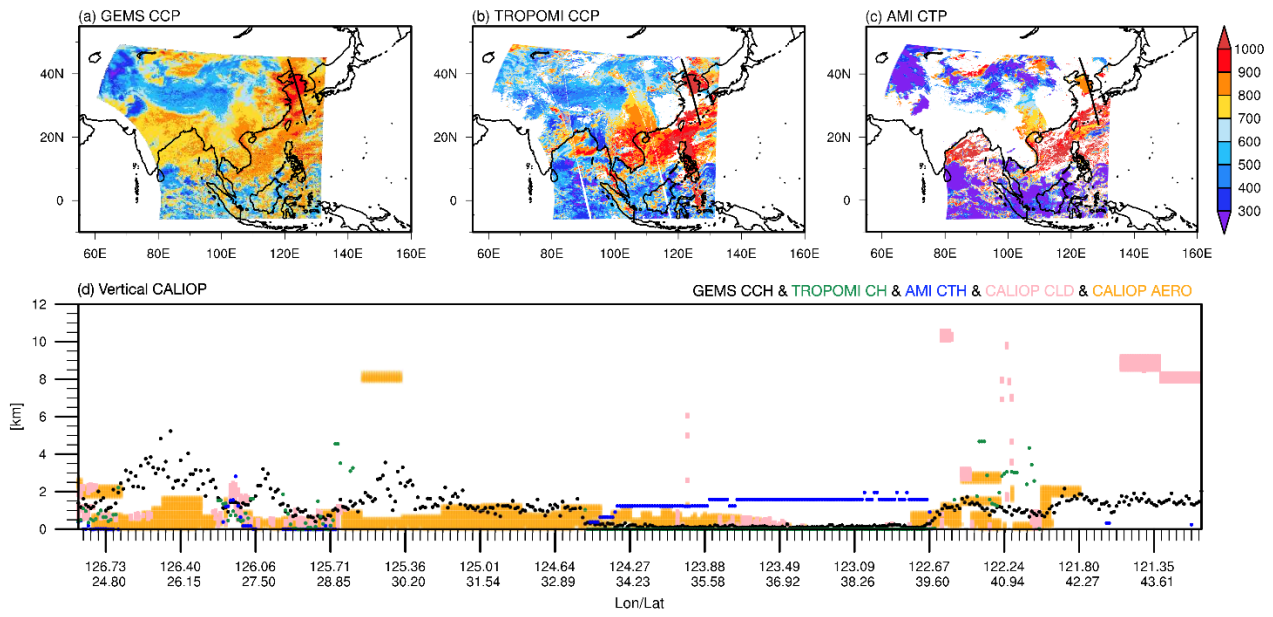
Figure 11: Sea fog on March 25, 2021. (a) CCP obtained from GEMS. (b) mCP from TROPOMI. (c) CTP derived from AMI. (d) CHs converted to cloud altitude from three satellites overlaid onto the CALIOP VFM image.